JOURNAL OF MATERIALS SCIENCE 32 (1997) 6539–6547

Rubber particle size and cavitation process in high impact polystyrene blends

C. A. CORREA, J. A. de SOUSA*
*Centro de Caracterização e Desenvolvimento de Materiais, and *Materials Engineering Department, Universidade Federal de São Carlos, Via Washington Luiz, Km 235-13565-905-São Carlos SP, Brasil*

The rubber particle size and its volume fraction are recognised as being important factors in determining the yield and fracture behaviour of high impact polystyrene (HIPS). However, correlations between the average particle size and cavitation in the rubber with toughening efficiency have only recently been established theoretically. This work provides further evidence on how the deformation kinetics in HIPS are affected by variations in the average rubber particle size highlighting along the way the role of rubber cavitation in the process. Variations in the average particle size were achieved by melt blending different proportions of two commercial grades of HIPS that had the traditional multiple inclusion particle morphology. Tensile and impact properties of the blends were measured and correlated to morphological parameters determined by quantitative image analysis. It was found that yield and fracture behaviour in tensile and impact test were strongly dependent on the amount of sub-micron particles in the blend. At high rates, toughness drops steeply with particle size. It was proposed that stress at yield and post yield strain hardening are controlled by particle size and rubber stretching respectively. Microfracture analysis by transmission electron microscopy lent support to the arguments presented.

1. Introduction

The tendency of many polymers to undergo brittle failure, especially in notched impact tests, has made the rubber toughening of plastics and its relationship with polymer composition and morphology a major issue in polymer science. In general, the fracture resistance of glassy and brittle polymers, can be markedly improved by incorporating a dispersed rubber phase. This important industrial procedure leads to a class of materials named rubber toughened plastics (RTP's). Well known commercial examples in large use are high impact polystyrene (HIPS) and acrylonitrile–butadiene–styrene terpolymer (ABS). A number of factors, related to rubber component, have been identified as affecting the toughness of these systems. These factors include the volume fraction of the rubber phase, its chemical composition, degree of crosslinking, particle morphology, adhesion to the matrix and the rubber particle size and its size distribution [1].

1.1. Morphological aspects in rubber toughening

Recent advances in polymer chemistry have allowed the manufacture of rubber toughened plastics with different kinds of rubber morphology. In the particular case of HIPS, the rubber phase is a composite structure consisting of bulk rubber with polystyrene (PS) subinclusions. In most cases the rubber used is polybutadiene (PBd) although SBR and EPDM are also recommended according to the intended application. Particle size and morphology are determined during the phase inversion in the polymerization process and mass polymerization tends to lead to a quite broad distribution of multiple inclusion particles. On the other hand, emulsion polymerization leads to the so-called *onion* or core-shell structures, usually from block copolymers of styrene–butadiene–styrene, which present a smaller particle size and a less dispersed distribution. Another physical method used for controlling the morphology and at the same time improving interface properties, is the addition of block co-polymers to the system. Depending on their composition, chemical structure and dispersion conditions, different types of particle morphology can be attained, as has been reviewed by Echte [2].

The effects of the average rubber particle size on the toughness of rubber modified polymers have been reviewed by Wu [3], who commented on the contradictory information to be found in the literature. While in polymers such as HIPS an increase in toughening is attained by increasing the average particle size, in ductile polymers such as polyamides and polycarbonates, a higher toughness correlates with a decreasing average particle size and particularly to the interparticle distance, Wu [4, 5] and Borggreve *et al.* [6]. Therefore, the best approach is to present

0022–2461

a maximum in toughness associated with an optimum particle size range. In HIPS this has been quoted to be 2–5 μm, Bucknall [1]; Donald and Kramer [7] and Cigna *et al.* [8].

Although it is very difficult to isolate the particle size effect on toughening – without changing other factors such as rubber morphology, crosslinking and particle-matrix interface – in recent studies by Cook *et al.* [9] on latex modified polystyrene with monodispersed particle distributions no toughening was found below 2 μm in particle diameter. Also, according to the authors, an optimum impact strength in monodispersed particle size HIPS is found in the region of 2–3 μm at 8 wt % rubber content in the mixture.

The particle size distribution or the particle size spectrum has also been related to toughening efficiency, Hobbs [10]. Optimization of the particle size and particle size distribution, such as in blends with bimodal particle distributions, were suggested to improve toughening in HIPS by Okamoto *et al.* [11], and rubber toughened epoxies by Kinloch and Houston [12]. The advantages due to reducing particle size without lowering the impact strength are related to gloss and transparency properties of RTP's in general regarding the toughening process operating in the material.

1.2. Rubber cavitation

Early studies of rubber toughening in polymers have highlighted a close relationship between the magnitude of the hydrostatic pressure on the particle and its shear modulus, Bragaw [13]. Basically the source of the hydrostatic stress is the difference in the Poisson's ratio between the rubber and the matrix (rubber ≈ 0.5 and matrix ≈ 0.4), although thermal misfit, which is related to differences in the thermal coefficients of the matrix and the rubber, can also contribute to the hydrostatic stress. Further, although the shear modulus of the rubber can be negligible in comparison to that of the matrix, the rubbery inclusion could still support a significant negative pressure (G) due to its high bulk modulus (K) (For polybutadiene; $G \approx 0.62$ GPa and $K \approx 1.94$ GPa), Boyce *et al.* [14].

More recent studies of nylon-rubber blends have shown that the stress fields surrounding rubber particles are hardly affected by the mechanical properties of the elastomer, and are more likely to be explained by differences in cavitation stresses of different types of rubber, Dijkstra [15]. This effect has also been reported in HIPS and PS-PBd block copolymers irradiated with gamma rays. Gamma radiation seems to increase the crosslink density in the rubber and consequently changes the matrix yield properties, Schwier *et al.* [16] and Birkinshaw *et al.* [17].

Following those findings, an energy-balance criterion for rubber cavitation in RTP's was advanced by Lazzeri and Bucknall [18]. Their model was based on the fact that the rubber cavitation should be governed by the particle volume strain and a balance between stored volume energy, void surface energy, and the work required to stretch the rubber surrounding the void biaxially. Accordingly, rubber cavitation should become unlikely with a decreasing particle size and an increasing rubber crosslink density. Further refinements in the model, accounting for morphological aspects, have been presented in two recent papers by Bucknall and co-workers [19, 20]. In line with these findings. Guild and Young [21] have suggested that the hydrostatic stresses required for rubber cavitation in rubber modified epoxies is dependent on the void size and may vary from 0.4 to 40 MPa for 0.1 and 0.01 μm voids, respectively.

The idea of rubber particle cavitation in rubber toughened systems is now becoming more accepted with recent advances in rubber toughening research. To complement the theoretical basis, electron microscopy has provided further evidence that craze phenomena in HIPS is usually related to rubber cavitation [31]. The observations suggest that rubber particles in RTP's are not only mere stress concentrators – as suggested by many studies based on finite element analysis – but rubber cavitation during the deformation process that leads to a relief of triaxial stress with extensive yielding in the surrounding matrix. This is particularly evident ahead of notches where the size of a whitening zone can be related to the ability of the rubber component to balance the high strains in the surrounding matrix after it has cavitated, Schwier *et al.* [22]. It is also currently accepted that the effect of rubber particle size itself correlates with matrix ductility and that the rubber intrinsic properties play an important role if cavitation of the rubber determines the yield conditions in the matrix. Independent of the rubber toughening mechanism, rubber particle cavitation has been identified in many RTP's, including PVC, Breuer *et al.* [23], rubber modified epoxies, Yee and Pearson [24, 25], and nylon rubber blends, Ramsteiner and Heckmann [26], Borggreve *et al.* [6], Bucknall *et al.* [27] and Speroni *et al.* [28]. In the literature, cavitated particles in HIPS are often reported in connection with crazes, while in nylon rubber blends, voiding in the rubber phase should be more closely related to localized shear bands.

A key experiment carried out by Bubeck *et al.* [29] using **r**eal-**t**ime **s**mall **a**ngle **X**-ray **s**cattering (SAXS) in tensile impact testing, shed some light on the controversial subject of deformation mechanisms in RTP's. They found that a substantial volume increase observed in tensile loading is due to cavitation within rubber particles, which in many RTP's precedes multiple crazing and/or shear yielding in the matrix. These findings contradict many previous conclusions based on volumetric dilatational analysis which regarded deformation and yielding in HIPS as occurring basically by crazing rather than any other micromechanism.

After the SAXS experiments, the real sequence of events leading to crazing and failure in HIPS has been reopened for investigation. In this work more evidence is presented to confirm that rubber cavitation is actually determined by particle size and that it should be preceded by crazing in the matrix. After rubber

cavitation, the elastic energy stored within the particle is released once a critical strain volume is attained. We propose that many aspects of this sequence of events can be derived from a typical stress–strain plot in a tensile test. On this basis, yield stress would be determined by average particle size while post-yield strain hardening should be related to rubber stretching and stiffening, using concepts of the non-linear rubber elasticity theory. Therefore, the rubber is regarded as a load-bearing structure – rather than mere stress concentrators – sharing a substantial part of the load with the matrix. In our study, correlations between the effect of average particle size and its volume fraction on the tensile and impact properties of HIPS is fully investigated and discussed in the light of the new developments in the field.

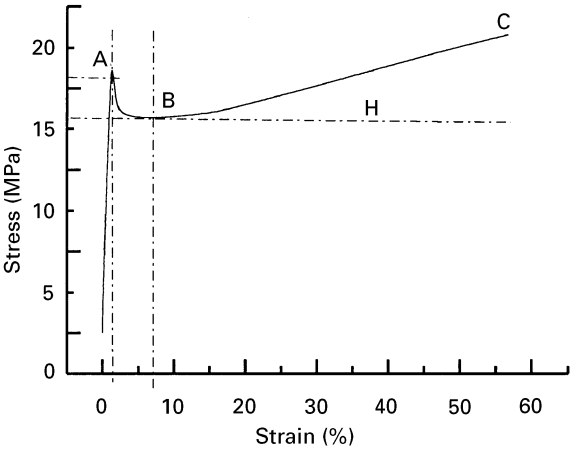

Figure 1 A typical stress–strain plot for HIPS in uniaxial tension illustrating the main parameters obtained from the tests. A (σ_{hy} = higher yield); B (σ_{ly} = lower yield or flow stress); C (σ_f = fracture) and H (strain hardening).

2. Experimental details

2.1. Materials

Two commercial grades of HIPS supplied by Dow Chemical, Netherlands and Basf, Germany, H472 and H576H respectively were chosen as the parental compositions for this study. The choice considered differences in rubber particle average size and distribution, while the particle internal morphology was the same – the well characterized multiple inclusion or *salami* particles. Image analysis of scanning electron microscopy (SEM) micrographs were used to characterize the selected grades in terms of their rubber particle *apparent* volume fractions, Φ_A, and particle average diameter, D_n.

Variations in the average rubber particle size, the shape of the particle spectrum and particle volume fraction were achieved by blending both the HIPS and a standard PS grade for extrusion (Basf 143-E) at varying Φ_A levels. These values were determined nominally, i.e., by considering the determined particle volume fraction in the parental compositions and the weight per cent of each component plus the polystyrene added. The processing was carried out in a *Leistritz* 30 mm co-rotational twin screw extruder at 10 r.p.m. and barrel temperatures ranging 195 to 220 °C along 8 zones.

After being compounded all the HIPS compositions were injection moulded into standard ASTM D638 type I specimens for tensile testing. Sheets of 6 mm thickness were compression moulded at 200 °C in a 20 min cycle including 10 min for homogenizing. The moulding was completed by switching off the power and allowing the plates to cool down naturally to room temperature. The sheets were used in the preparation of notched bars for impact tests according to ASTM D256.

2.2. Uniaxial tensile tests

The main parameters from tensile tests were determined from stress–strain diagrams, as shown in Fig. 1. The equipment for testing was a fully automated Instron IX series machine. The tests were performed using a crosshead speed of 10 mm min^{-1} in a controlled room temperature of 23 °C. Tests at a constant stress rate of 10 MPa min^{-1} were also performed for the two basic HIPS used as parental compositions in this study. An average of 10 specimens were taken for each sample.

The lower yield, σ_{ly}, has been taken to be the flow stress of polystyrene fibrils after a craze has been formed but has not yet been fully extended to its maximum draw ratio. The term strain hardening, H, is related to the increase in stiffness observed after yield with increasing deformation and it is given by the slope of the post-yield stress–strain curve.

2.3. Instrumented impact tests

The test consists of hitting the upper position of a vertically clamped v-notched specimen with a standard instrumented hammer. The impact strength is obtained in terms of the energy absorbed by the specimen, in Joules, which is divided by the specimen thickness in the notch region (J m^{-1}). Diagrams of force versus displacement are used to calculate the energy for crack initial growth (taken at the maximum force) and fracture (area under the curve or total energy). The equipment used to evaluate the impact strength was an instrumented pendulum from Ceast model Resil 50, configured for IZOD testing according to ASTM D256.

The main set-up parameters were defined according to the materials fracture behaviour and are listed in Table 1.

The specimen dimensions followed the ASTM D256-Method A for single edge notched bars of size $60 \times 12 \times 6$ mm. The impact conditions were defined in terms of energy and velocity according to the hammer height. An average of five specimens were tested for each sample while the results were presented in terms of force and energy versus time diagrams.

2.4. Morphological and fracture analysis

The morphological parameters were determined by quantitative image measurements in terms of average particle size and volume fraction. Cryo-fractured and

TABLE I Main set up parameters used in instrumented impact tests

	Neat polystyrene	HIPS-PS blends
Number of points	500	50
Sampling time (μs)	5.0	8.0
Test time (μs)	2.5	4.0
Strike range (kN)	3.600	3.600
Working range (kN)	3.600	3.600
Hammer mass (kg)	0.670	0.670
Hammer length (m)	0.330	0.330
Starting angle (deg)	40	63
Impact velocity (m s^{-1})	1.23	1.88
Energy (J)	0.51	1.18

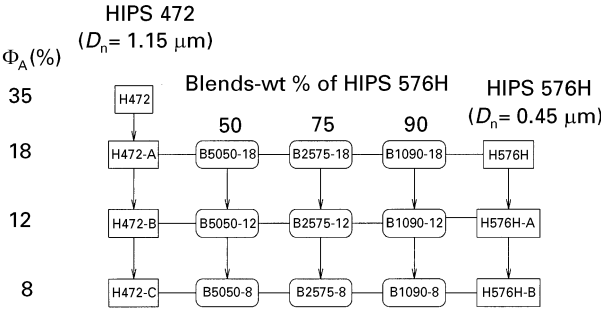

Figure 3 Schematic diagram showing HIPS blends composition prepared in a Leistritz co-rotational twin screw extruder.

cromic acid etched surfaces of the parental compositions were used in sample preparation. Quantitative measurements were performed using a Leica Quantiment 600 image analyser. Fracture analysis in regions around the crack tip of the notched bars after impact were performed in order to investigate the toughening mechanism in the damaged area. Ultrathin films from these areas were prepared in a RMC ultramicrotome. Blocks from compression moulded plates were stained with osmium tetraoxide. The films were aproximately 100 nm thick and were observed in a Zeiss 912 Omega energy filtering transmission electron microscope (EF-TEM).

3. Results and discussion

3.1. SEM characterization and quantitative particle analysis

In Fig. 2 (a and b) the typical morphologies of H472 and H576H are illustrated as observed by scanning electron microscopy of cryofractured and etched surfaces. The corresponding histograms of the particle diameter distribution are depicted in Fig. 2c and d.

According to Fig. 2(a–d) the results of the particle analysis were $\Phi_A = 35\%$ and $D_n = 1.15$ μm for HIPS H472 and $\Phi_A = 18\%$ and $D_n = 0.45$ μm for HIPS 576H. These values have been used as a reference to derive the compositions shown in Fig. 3.

3.2. Tensile properties

The tensile properties of the HIPS were first investigated by considering the variations in volume fraction of two HIPS grades after blending the two parental compositions with the neat polystyrene. The results are summarized in Table II for both HIPS 472 and 576H diluted series. The corresponding stress–strain diagrams are depicted in Fig. 4 (a and b).

Considering that previous studies have shown no major changes in the particle spectra of HIPS-PS

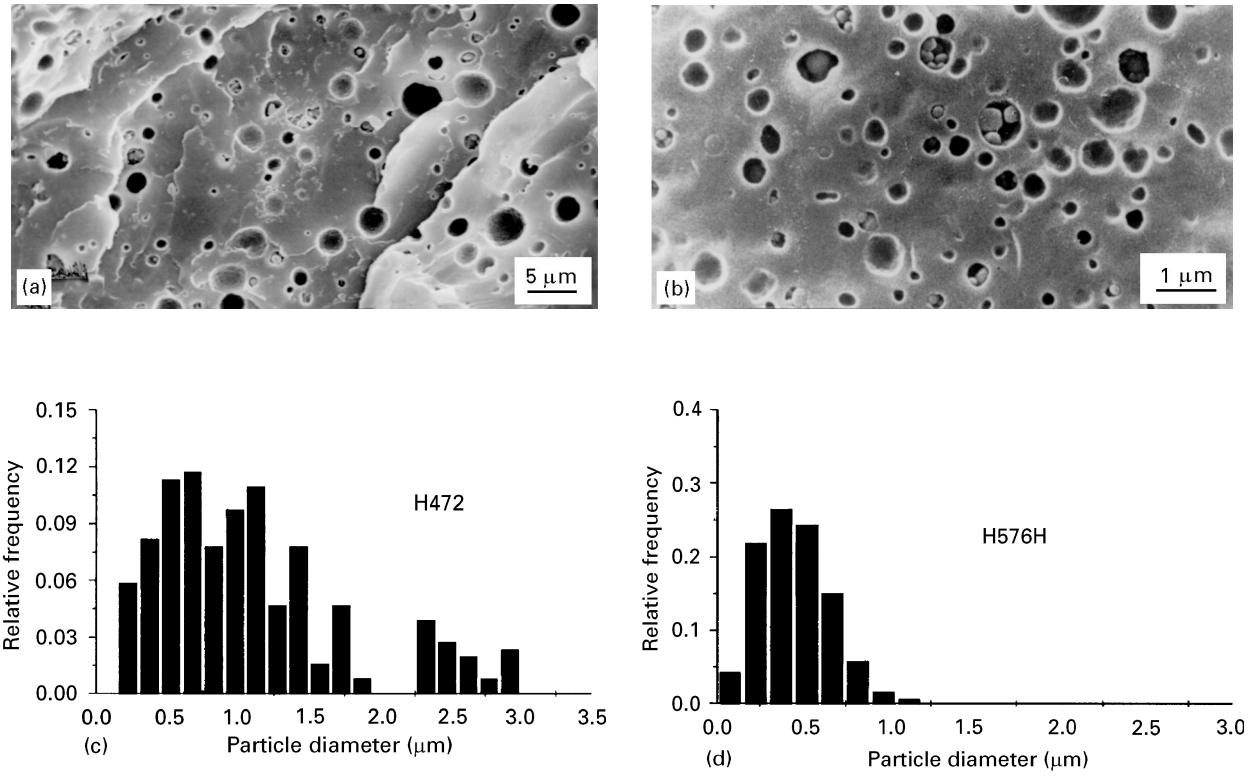

Figure 2 SEM cryo-fractured and etched surfaces with corresponding particle size histogram of the two parental HIPS grades.

TABLE II The effect of volume fraction on the tensile properties of HIPS H472 and 576H diluted series

HIPS-472 $D_n = 1.15$ μm	σ_{hy} (MPa)	ε_{hy} (%)	σ_{ly} (MPa)	ε_{ly} (%)	σ_f (MPa)	ε_f (%)	E (GPa)
$\Phi_A = 35$	16.16 ± 0.11	1.31 ± 0.04	13.25 ± 0.10	6.30 ± 0.83	18.31 ± 0.47	56.83 ± 4.81	1.79 ± 0.16
$\Phi_A = 18$	21.69 ± 0.40	1.16 ± 0.04	16.57 ± 0.19	4.91 ± 0.29	20.70 ± 0.20	38.99 ± 0.91	2.17 ± 0.09
$\Phi_A = 12$	25.03 ± 0.39	1.18 ± 0.05	18.33 ± 0.27	4.56 ± 0.40	21.98 ± 0.23	31.12 ± 1.81	2.40 ± 0.18
$\Phi_A = 8$	27.74 ± 0.42	1.22 ± 0.02	19.79 ± 0.26	4.36 ± 0.26	23.23 ± 0.20	27.34 ± 1.81	2.70 ± 0.15
HIPS-576H $D_n = 0.45$ μm	σ_{hy} (MPa)	ε_{hy} (%)	σ_{ly} (MPa)	ε_{ly} (%)	σ_f (MPa)	ε_f (%)	E (GPa)
$\Phi_A = 18$	25.11 ± 0.36	1.39 ± 0.06	18.96 ± 0.22	11.21 ± 1.90	19.95 ± 0.52	26.22 ± 8.45	1.99 ± 0.09
$\Phi_A = 12$	27.58 ± 0.31	1.38 ± 0.04	20.19 ± 0.17	10.42 ± 0.92	21.05 ± 0.34	27.07 ± 2.33	2.25 ± 0.11
$\Phi_A = 8$	29.05 ± 0.85	1.39 ± 0.06	21.25 ± 0.40	7.97 ± 0.98	22.31 ± 0.37	26.09 ± 2.49	2.96 ± 0.22

ε_{ly} = lower yield or strain at flow stress; ε_f = strain at failure

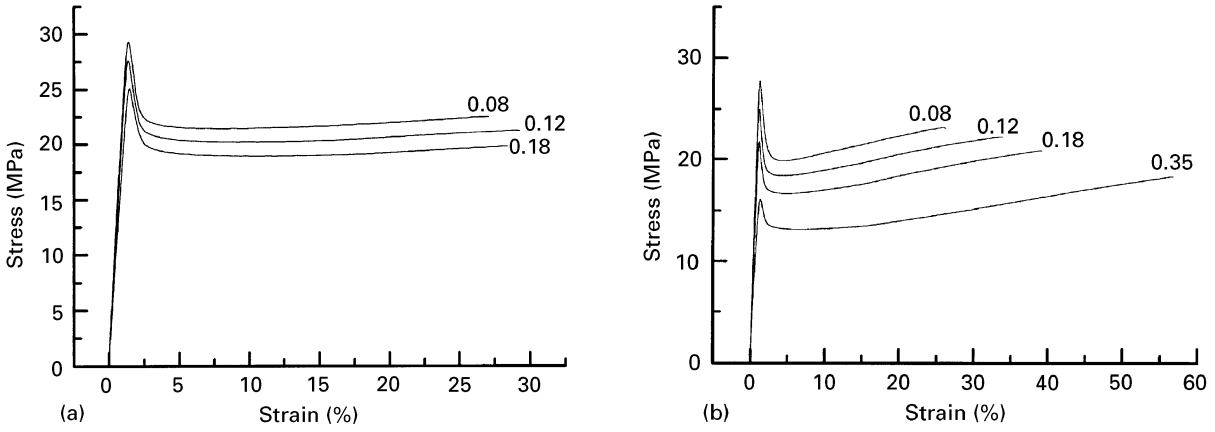

Figure 4 (a) The effect of Φ_A on the tensile plots of HIPS 576H blended with neat PS and (b) the effect of Φ_A on the tensile plots of HIPS 472 blended with neat PS.

diluted series by melt blending [29], the effect of changes in the average particle size on tensile properties were also investigated by testing blends of HIPS 472/576H/PS at different HIPS proportions and particle volume fractions. Accordingly, the variations in average particle size shown in Table III were calculated in terms of average particle size in the parental compositions and weight proportions of each component in the blend. In spite of this approximation, the results shown in Table III were quite consistent with those shown in Table II.

The main differences presented in the tensile diagrams are related to average particle size and rubber particle volume fraction. Fig. 4 (a and b) show that the yield stress (σ_{hy}), flow stress (σ_{ly}), and yield strain (ε_{hy}) are increased by reducing the average particle size independently of the rubber particle volume fraction. Analogously, within HIPS blends, as the amount of small particles is increased the same trend is observed at equivalent levels of Φ_A (Table III). These results are consistent with observations reported by other authors for HIPS [29] and also recent studies in rubber toughened polyamides carried out by Borggreeve *et al.* [6] that correlated an increase in yield stress to the inability of small particles to cavitate in the same deformation levels of large particles. Such evidence would also explain the increase in yield strain, (ε_{hy}), with decreasing average rubber particle size as shown in Table II for HIPS diluted series. An equivalent value of ε_{hy} for all tensile plots independent of Φ_A in the HIPS dilution series suggests that the average particle size, i.e. a critical particle volumetric strain, determines whether or not cavitation takes place. According to the energy-balance cavitation criterion proposed by Bucknall *et al.* [20], changes in the particle volume strain depend on the particle size and they correlate with the stored energy required to overcome the surface tension to form a microvoid in the rubber. Thus, by reducing the particle size, the change in particle volume strain required to produce a stable void is higher as suggested by a decrease in the yield stress with average particle size. However, the fracture stresses, σ_f, for both HIPS diluted series remain at the same levels implying that fracture in HIPS might be related to the failure in the rubber (Tables II and III; Fig. 5).

On the other hand, the strain at failure ε_f is a function of Φ_A and at high particle concentrations it increases with increasing average particle size. However, for HIPS 472/576H blends, differences in ε_f tend to become independent of the average particle size at lower Φ_A as is depicted in Fig. 6.

By comparing the two tensile diagrams shown as Fig. 4 (a and b) it is clear that the strain hardening effect is more pronounced in HIPS with a larger average particle size (HIPS 472 diluted series). Assuming

TABLE III The effect of average particle size on the tensile properties of HIPS 472/576H/PS blends

Blends 472/576H[a]	σ_{hy} (MPa)	ε_{hy} (%)	σ_{ly} (MPa)	ε_{ly} (%)	σ_f (MPa)	ε_f (%)	E (GPa)
B5050-18 ($D_n^* = 0.80$ μm)	22.63 ± 0.10	1.25 ± 0.09	17.72 ± 0.07	5.53 ± 0.65	20.60 ± 0.41	39.60 ± 4.54	2.01 ± 0.10
B2575-18 ($D_n^* = 0.62$ μm)	23.61 ± 0.51	1.38 ± 0.07	18.36 ± 0.29	7.26 ± 0.95	19.98 ± 0.17	33.61 ± 1.71	2.12 ± 0.13
B1090-18 ($D_n^* = 0.52$ μm)	24.09 ± 0.10	1.40 ± 0.06	18.60 ± 0.06	11.47 ± 1.23	19.45 ± 0.28	27.70 ± 4.06	2.29 ± 0.09
B5050-12 ($D_n^* = 0.80$ μm)	25.50 ± 0.22	1.25 ± 0.05	19.36 ± 0.17	5.74 ± 0.59	21.60 ± 0.26	33.11 ± 1.89	2.70 ± 0.20
B2575-12 ($D_n^* = 0.62$ μm)	25.81 ± 0.26	1.26 ± 0.02	19.46 ± 0.15	6.84 ± 0.8	20.93 ± 0.28	28.39 ± 2.71	2.62 ± 0.12
B1090-12 ($D_n^* = 0.52$ μm)	26.20 ± 0.10	1.28 ± 0.07	19.78 ± 0.09	8.46 ± 1.30	21.08 ± 0.11	30.36 ± 0.88	2.61 ± 0.21
B5050-8 ($D_n^* = 0.80$ μm)	28.34 ± 0.31	1.23 ± 0.03	20.80 ± 0.11	5.04 ± 0.52	22.87 ± 0.52	28.32 ± 1.21	3.05 ± 0.13
B2575-8 ($D_n^* = 0.62$ μm)	29.00 ± 0.14	1.27 ± 0.03	21.23 ± 0.10	6.04 ± 0.90	22.85 ± 0.15	26.91 ± 2.06	3.02 ± 0.09
B1090-8 ($D_n^* = 0.52$ μm)	29.39 ± 0.19	1.29 ± 0.05	21.40 ± 0.16	6.56 ± 0.7	22.55 ± 0.12	25.25 ± 1.07	3.11 ± 0.15

[a] BXXYY-Φ_A-B = Blend; XX = wt% of HIPS 472; YY = wt% of HIPS 576; Φ_A = Apparent particle volume fraction; D_n^* = Estimated average particle diameter

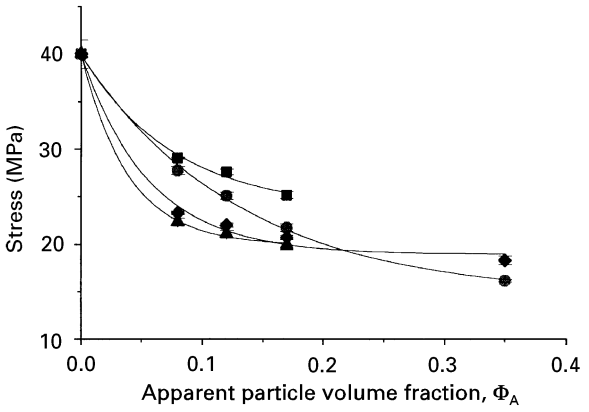

Figure 5 Variation in stress at yield and fracture with volume fraction Φ_A for HIPS 472 and 576H diluted series. Key: (■) H576H-yield, (●) H472-yield, (▲) H576H-fracture and (◆) H472 fracture.

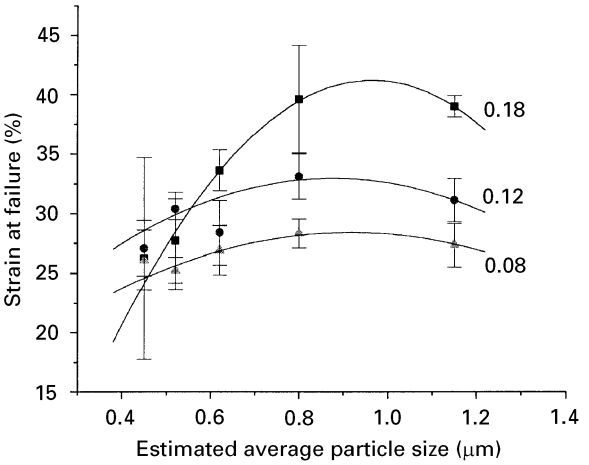

Figure 6 Variations on the strain at failure with estimated average particle diameter and particle volume fraction Φ_A for HIPS 472 and 576H blends.

that the strain hardening is introduced by rubber stretching after yield, at failure the applied load is shared between the matrix and the stretched rubber. A simple relationship to account for the amount of load transfered from the matrix to the particle can be expressed as follows:

$$\sigma_f = \sigma_{PS}(1 - \Phi_A) + \sigma_R(\Phi_A) \quad (1)$$

where σ_f = stress at failure; $\sigma_{PS} = \sigma_{ly}$ and σ_R = stress in the rubber.

Substituting the values in Table II for HIPS 472 (Fig. 4b) into Equation 1, the failure stress in the rubber can be calculated to vary from 5 to 9 MPa depending on Φ_A. These estimates comply with recent developments in rubber toughening research, where the rubber component is regarded as being a load bearing element, rather than a mere stress concentrator, withstanding a substantial part of the load as the deformation increases. The characteristic stress–strain behaviour of the rubber can be simulated using non-Gaussian expressions such as the inverse Langevin function thereby accounting for the effects of the rubber crosslink density and shear modulus shown in the rubber stress–strain diagrams [31].

Further evidence, for the suggested behaviour, can be obtained by comparing the values of ε_f found for HIPS in the HIPS 472 and 576H diluted series at equivalent levels of Φ_A (Fig. 6). From this comparison it is clear that the failure in HIPS is basically due to a collapse of rubber fibrils that is independent of the rubber particle size. Recent studies using irradiated samples of HIPS have shown that an increase in the rubber crosslink density, produced by an increase in the radiation dose, tends to increase the yield and flow stresses and reduce the strain at failure by suppressing the cavitation in the rubber [19]. Accordingly, rubber extension is constrained by reducing the particle size and increasing the rubber

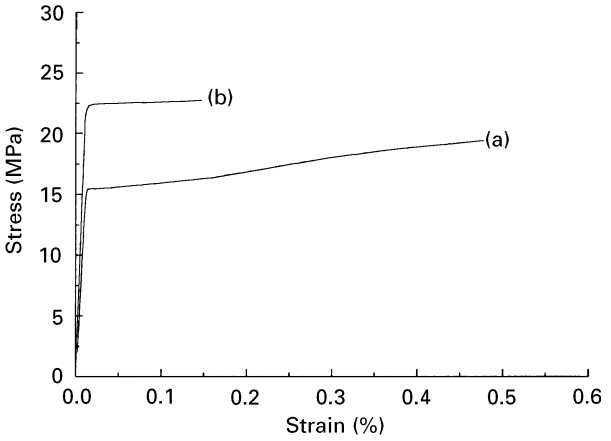

Figure 7 Effect of constant stress rate loading on stress–strain diagrams of (a) HIPS 472 and (b) HIPS 576H. Stress rate = 10 MPa min^{-1}

crosslink density, which tends to increase the yield stress and suppress the characteristic strain hardening after yield. This suggests that strain hardening induced by rubber stiffness is limited by the rubber stress at failure.

The results of tensile tests at a constant stress rate have provided further support for the arguments presented above and illustrate the main differences in the kinetics of deformation related to particle size in HIPS. Fig. 7 shows that the HIPS 576H grade with a smaller average particle size exhibits a much higher yield stress, with a much lower strain at failure than the HIPS 472 that has double the average particle size. Further, the suppression of strain hardening in HIPS 576H at stresses higher than those verified in HIPS 472 reinforces the point that rubber may fail before being extended.

3.3. Impact properties

The main aspects observed in the impact diagrams are basically those related to the amount of energy absorbed after the maximum force has been achieved. In typically brittle materials such as neat polystyrene there is a steep drop in the energy after the peak (Fig. 8a). However, in efficiently toughened samples such as the HIPS 472 a gradual drop in the energy absorbed with time was observed following extensive whitening along the crack path (Fig. 8b). The samples with a lower average particle size, HIPS 576H and the blend B1090, show a brittle–ductile transition with crack propagation in several stages. Thus, in these

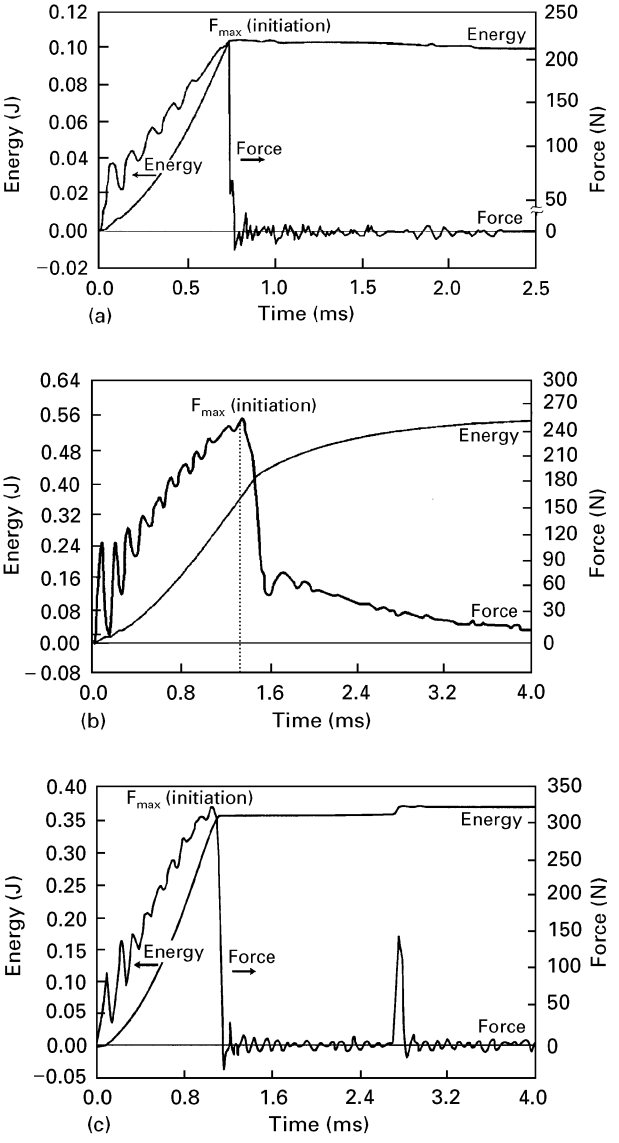

Figure 8 Force and energy versus time plots for (a) polystyrene, (b) HIPS 472 and (c) HIPS 576H (notched bars with 6 mm thickness).

compositions, despite the energy drop to zero after the peak, there was a slight increase in energy related to a transient stress whitening before complete failure (Fig. 8c).

The results of the instrumented impact tests are summarized in Table IV. The samples with equivalent Φ_A illustrate the effect of particle size distribution on the energy for initial crack growth and total failure.

Most importantly the peak energy, or the energy required for the initial crack growth does not seem to

TABLE IV Results of instrumented impact tests-Resil 50-Ceast ASTM D256-A (23 °C)

Sample (D_n)	Maximum force (N)	Initiation energy (J m^{-1})	Fracture energy (J m^{-1})
Polystyrene	205.56 ± 7.36	11.67 ± 2.93	13.33 ± 3.33
H472-35 (1.15 μm)	260.70 ± 13.20	60.00 ± 3.60	91.67 ± 5.50
H472-17 (1.15 μm)	311.70 ± 11.12	50.00 ± 3.35	83.33 ± 5.83
H576-18 (0.45 μm)	304.56 ± 19.69	53.33 ± 6.69	58.33 ± 10.49
B5050-18 (0.80 μm)	309.96 ± 17.33	55.00 ± 6.60	96.67 ± 12.56
B2575-18 (0.62 μm)	302.76 ± 11.76	48.33 ± 3.33	78.33 ± 5.40
B1090-18 (0.52 μm)	313.56 ± 16.00	50.00 ± 1.67	60.00 ± 2.54

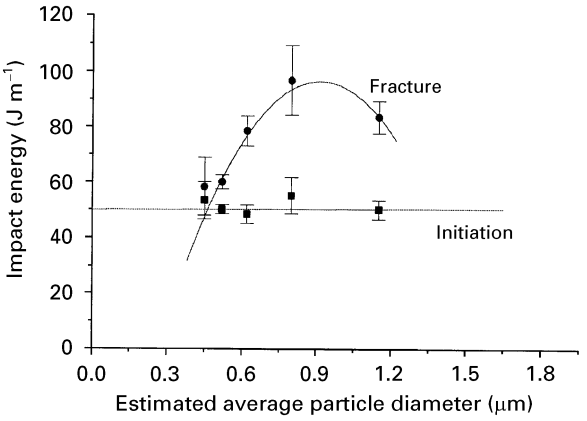

Figure 9 Diagram showing the variation of the energy absorbed in the impact tests as a function of estimated average particle size in HIPS 472 and 576H blends ($\Phi_A = 18\%$) ASTM D256-A (23 °C).

vary extensively with morphology within the range of samples tested (Fig. 9).

The impact tests disclose important information about the dependence of the particle size distribution on the kinetics of deformation, particularly at very high rates. The results shown in Fig. 9 suggest that the efficiency of the rubber toughening process is strongly related to the material's ability to withstand crack growth after maximum load. Thus, while in "quasi static" tests such as the uniaxial tensile test the stress at yield tends to increase linearly with decreasing average particle size, at high rates there is a brittle–ductile transition that is clearly related to the average particle size. The brittle–ductile transition is a very important process in rubber toughened plastics and should be monitored with respect to temperature.

3.4. Fracture analysis

The TEM micrographs presented in Fig. 10 (a and b) lend support to the arguments discussed in earlier sections. According to the micrographs, the crazing process in HIPS blends are more likely to be associated with larger particles as illustrated for blend B1090-18. The pictures suggest that the crazes may have been triggered after the stored elastic energy was relieved in the matrix by cavitated particles. This fits our proposed mechanism that a critical volumetric change of the particle has to be attained before cavitation takes place. Thus, sub-micron particles tend to cavitate in the later stages of deformation thereby assuming a more passive role as energy absorbers rather than toughening precursors. Actually, by forming an interconnected network of particles and crazes the structure may remain stable before any craze collapses. In this case, the average particle size and test speed settle the conditions for the occurrence of the brittle–ductile transitions. These results are in line with the results of the mechanical properties that correlated the yield and fracture with the average particle size and test conditions, i.e., uniaxial tension and impact. The study, carried out in HIPS with only multiple inclusion particles, reinforces earlier findings using bimodal systems with varying particle morphology [31].

4. Conclusions

The present work yields further insights into the role of rubber particles in the rubber toughening of HIPS. The study has shown that during tensile loading, the yield and failure processes are strongly related to the average rubber particle size which seems to be consistent with the ability of the rubber to cavitate. After yield, the rubber fibrils formed in the cavitated sites produce the observed strain hardening. The post-yield behaviour indicates that a substantial part of the load is being transferred from the matrix to the rubber at large deformations. The observations explain the relatively higher efficiency of large particles compared to sub-micron particles in toughening the PS matrix. The higher efficiency of large particles to toughen polystyrene is more evident for materials tested in impact. At high rates the large particles in the blend were responsible for the significant improvements observed in the energy absorbed at failure. EFTEM fracture studies carried out on these systems provided the data required to verify that the average rubber particle size in HIPS is the key factor for efficient rubber toughening of these materials.

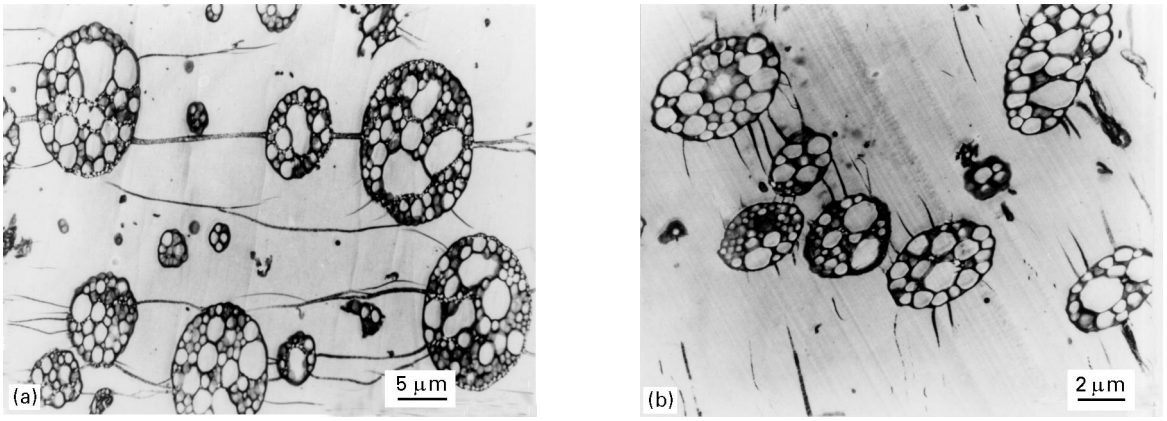

Figure 10 Evidence of rubber cavitation and crazing initiation in HIPS blends; (a) tensile specimen; (b) notch region of impacted specimen.

Acknowledgements

The authors thank the FAPESP agency in Brazil for financial support of this programme, the ICTPol – Instituto de Ciência e Tecnologia de Polímeros from Portugal for the blend processing, and the Polimate S/A for the impact test measurements.

References

1. C. B. BUCKNALL, "*Toughened plastics*" (Applied Science, London 1977).
2. A. ECHTE, in "*Rubber toughened plastics, advanced chemistry series 222*", edited by C. K. Riew (ACS, Washington, D.C., 1989).
3. S. WU, *Polymer* **26** (1985). 1855.
4. *Idem., J. Appl. Polym. Sci.* **35** (1988) 1549.
5. *Idem., Polym. Engng. Sci.* **30** (1990) 753.
6. R. J. M. BORGGREVE, R. J. GAYMANS and A. R. LUTTMER, *Makromol. Chem. Macromol. Symp.* **16** (1988) 195.
7. A. M. DONALD and E. J. KRAMER, *J. Appl. Polym. Sci.* **27** (1982) 3729.
8. G. CIGNA, P. LOMELLINI and M. MERLOTTI, *ibid.* **37** (1989) 1527.
9. D. G. COOK, A. RUDIN and A. PLUMTREE, *ibid* **48** (1993) 75.
10. S. Y. HOBBS, *Polym. Engng. Sci.* **26** (1986) 74.
11. Y. OKAMOTO, H. MYAGI and M. KAKUKO, *Macromol.* **24** (1991) 5639.
12. A. J. KINLOCH and D. L. HOUSTON, *J. Mater. Sci. Lett.* **5** (1986) 1026.
13. C. G. BRAGAW, in "*Multicomponent advanced systems, chemistry series 99*", edited by N. A. J. Platzer (ACS, Washington, D.C., 1971).
14. M. E. BOYCE, A. S. ARGON and D. M. PARKS, *Polymer* **28** (1987) 1680.
15. K. DIJKSTRA, PhD thesis, University of Twente, The Netherlands (1987).
16. C. E. SCHWIER, A. S. ARGON and R. E. COHEN, *Polymer* **26** (1985) 1985.
17. C. BIRKINSHAW, M. BUGGY and F. QUINGLEY, *J. Appl. Polym. Sci.* **48** (1993) 181.
18. A. LAZZERI and C. B. BUCKNALL, *J. Mater. Sci.* **28** (1993) 6799.
19. C. B. BUCKNALL, C. A. CORREA, V. L. SOARES and X. C. ZHANG, in *Proceedings of the 9th International Conference on Deformation, Yield and Fracture of Polymers*, Cambridge, April 1994 (Institute of Materials, London 1994).
20. C. B. BUCKNALL, A. KARPODINIS and X. C. ZHANG, *J. Mater. Sci.* **29** (1994), 3377.
21. F. J. GUILD and R. J. YOUNG, *ibid* **24** (1989) 2454.
22. C. E. SCHWIER, A. S. ARGON and R. E. COHEN, *Phil. Mag.* **52** (1985) 581.
23. H. BREUER, F. HAAF and J. STABENOW, *J. Macromol. Sci.-Phys.* **B14** (1977) 387.
24. A. F. YEE and R. A. PEARSON, *J. Mater. Sci.* **24** (1986) 2462.
25. *Idem., ibid.* **24** (1986) 2475.
26. F. RAMSTEINER and W. HECKMANN, *Polym. Commun.* **26** (1985) 199.
27. C. B. BUCKNALL, P. HEATHER and A. LAZZERI, *J. Mater. Sci.* **24** (1989) 2255.
28. F. SPERONI, E. CASTOLDI, A. FABBRI and T. CASARAGHI, *ibid.* **24** (1989) 2165.
29. R. A. BUBECK, D. J. BUCKLEY Jr., E. J. KRAMER and H. R. BROWN, *ibid.* **26** (1991) 6249.
30. C. A. CORREA, Caracterização de Polimeros Multifásicos. Parte 1: Processamento e Morfologia. *Revista Polímeros-Ciência e Tecnologia* (ABPOL) (1995).
31. C. A. CORREA, *PhD thesis*, Cranfield University, England (1993).

Received 5 July 1996
and accepted 22 May 1997